J Therm Spray Tech (2018) 27:1447–1464
https://doi.org/10.1007/s11666-018-0765-4

PEER REVIEWED

Non-transferred Arc Torch Simulation by a Non-equilibrium Plasma Laminar-to-Turbulent Flow Model

S. Mahnaz Modirkhazeni[1] · **Juan Pablo Trelles**[1]

Submitted: 7 June 2018 / in revised form: 18 September 2018 / Published online: 15 October 2018
© ASM International 2018

Abstract Non-transferred arc torches are at the core of diverse industrial applications, particularly plasma spray. The flow in these torches transitions from laminar inside the torch to turbulent in the emerging jet. The interaction of the plasma with the processing gas leads to significant deviations from local thermodynamic equilibrium (LTE) far from the arc core. The flow from a non-transferred arc plasma spray torch is simulated using a non-LTE (NLTE) plasma flow model solved by variational multiscale (VMS) and nonlinear VMS (VMS_n) methods, which are suitable for unified laminar and turbulent flow simulations. Non-plasma turbulent jet simulations indicate that the VMS_n method produces results comparable to those by the dynamic Smagorinsky method, often considered the workhorse for turbulent incompressible flow simulations. VMS and VMS_n approaches are applied to the simulation of incompressible, compressible, and NLTE plasma flows in non-transferred arc torch operating at representative conditions found in plasma spray processes. The NLTE plasma flow simulations reproduce the dynamics of the arc inside the torch together with the evolution of turbulence in the produced plasma jet in a cohesive manner. However, the similarity of results by both methods indicates the need for numerical resolution significantly higher than what is commonly afforded in arc torch simulations.

Keywords incompressible–compressible flow · non-transferred arc plasma torch · two-temperature model · turbulence · turbulent free jet · variational multiscale

Introduction

Non-transferred Arc Plasma Torches

Direct-current (DC) non-transferred arc plasma torches are at the core of diverse technological applications such as metallurgy, spheroidization, chemical and particle synthesis, waste treatment, and particularly plasma spraying. Non-transferred arc torches have been the workhorses of plasma spraying processes for a wide range of applications, particularly for the deposition of thermal barrier (about 25% of the plasma spray market) and wear-resistant coatings. Even though a great amount is known about the operation of non-transferred arc plasma torches thanks to numerous computational and experimental means (e.g., Ref 1, 14), the need for improved spraying process performance, efficiency, as well as novel technological developments, such as liquid and suspension plasma spraying, prompts the need for greater understanding of these devices. Physics-based computational models can provide insight into process characteristics practically inaccessible through experimental means, as well as guide equipment design and process development.

In non-transferred arc torches, the electrodes are inside the torch, and therefore, electric current does not get transferred between the torch and the workpiece. In DC non-transferred arc torches, an imposed current between a conical cathode and a surrounding anode establishes an electric arc that interacts with a stream of processing gas producing a plasma that emerges as a jet (Ref 1). Figure 1

✉ S. Mahnaz Modirkhazeni
seyedehmahnaz_modirkhazeni@uml.edu

Juan Pablo Trelles
Juan_Trelles@uml.edu

[1] Department of Mechanical Engineering, University of Massachusetts Lowell, Lowell, MA 01854, USA

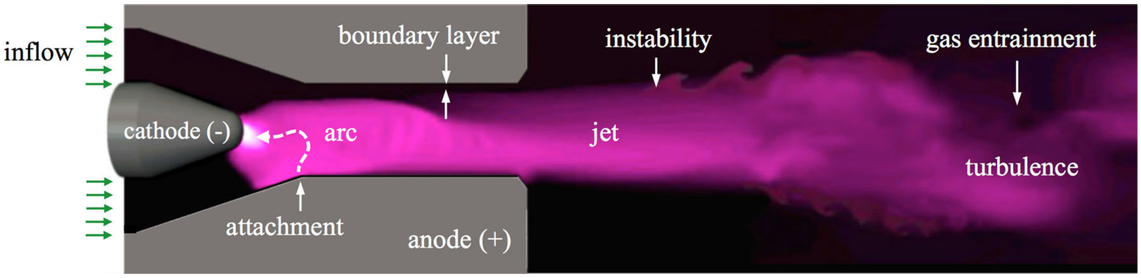

Fig. 1 Schematic representation of the flow from a direct-current non-transferred arc plasma torch

schematically depicts the flow through a DC non-transferred arc plasma torch indicating some of its key components and characteristics, i.e., the establishment of the arc following the current path, the formation of a cold boundary layer around the plasma, the development of shear instabilities, gas entrainment into the plasma stream, and the development of turbulence in the jet downstream.

Phenomena in Non-transferred Arc Torches

The plasma in non-transferred arc torches is typically considered as thermal plasma. Thermal plasmas are characterized by high collision frequencies among electrons and heavy species (molecules, atoms, ions), which cause them to be in a state of local thermodynamic equilibrium (LTE). Under LTE, all species share the same Maxwellian velocity distribution characterized by a single temperature (Ref 3). Nevertheless, the LTE state is generally found in the arc core only. The interaction of the plasma with its surrounding environment causes large variations in the degree of ionization, from non-ionized within the working gas to fully ionized in the plasma core, as well as large velocity, temperature, and density gradients. Such interactions cause significant deviations from LTE, leading parts of the flow to a state of thermodynamic non-equilibrium (non-LTE or NLTE). Under NLTE, electrons and heavy species have different Maxwellian velocity distributions (Ref 2-4) and therefore are characterized by different temperatures (Ref 5).

In addition to the occurrence of NLTE, the plasma flow in non-transferred arc torches experiences compound coupling among fluid dynamics, heat transfer, chemical kinetics, and electromagnetic phenomena. This multiphysics coupling leads to intricate flow dynamics and makes the flow inherently multiscale; that is, distinct phenomena are observed through different regions of the flow domain, e.g., from the thickness of boundary layers and plasma–gas interaction fronts, to the amplitude of instabilities along the jet. Moreover, the flow in arc torches is prone to the development of different types of instabilities, and it often transitions from laminar inside the torch to turbulent in the emerging jet.

Turbulent flow behavior enhances the exchange of species mass, momentum, and energy and therefore alters all intervening transport processes. The strength of turbulence in plasmas depends on their thermodynamic state (Ref 6); particularly, as indicated by Volkov (Ref 7), the amplitude of turbulence in plasmas increases as the plasma gets farther from thermodynamic equilibrium. From a practical perspective, turbulence in non-transferred arc torches can have a determining effect in the aimed process. Sometimes turbulence is desirable in processes such as surface treatments and nanoparticle synthesis (Ref 8) that benefit from the enhanced flow dissipation. For other processes, particularly for plasma spraying, the enhanced mixing from the surrounding environment caused by turbulence can lead to undesirable oxidation (Ref 9). Moreover, plasma–feedstock interactions are markedly important in emerging processes, particularly in liquid feedstock and suspension plasma spraying (Ref 10-13). The liquid-base droplets and resulting very fine particles are very sensitive to any perturbation in the jet, as they can drastically enhance mixing and heat transfer and therefore markedly affect the evolution of droplets and particles and their subsequent transfer by condensation into the coating. An overview of the challenges in understanding brought forward by novel and emerging plasma spray technologies, particularly of the interaction between the plasma flow and the feedstock, is discussed in the review article by Vardelle et al. (Ref 10).

Significant understanding related to turbulence in arc plasma torches has been achieved to date. For instance, Pfender et al. (Ref 11) experimentally investigated the turbulent structures of DC thermal plasma jets. They observed that the plasma core is generally not turbulent (i.e., laminar), whereas shadowgraphs revealed significant turbulence in the jet enhanced by fluctuations of the jet core due to the arc dynamics. Hlína and Šonský (Ref 12-15) investigated the dynamic behavior of the core of a plasma jet using three-dimensional optical diagnostics and image-processing techniques. Complementing experimental observations, numerical findings have revealed that high-temperature plasma regions exhibited less turbulent structures with large eddies (i.e., coherent regions with high vorticity), whereas low-temperature regions tend to be more turbulent with numerous small eddies. Shigeta (Ref 8) showed that the turbulent nature of the emerging plasma jet depends on the dynamics of the arc inside the torch, which cause major fluctuations in the jet core, and that the high temperature of the plasma produces a re-laminarization effect. Therefore, comprehensive arc plasma torch simulations have to be able to reproduce the transition from laminar flow inside the torch to turbulent flow in the plasma jet naturally, that is, as a consequence of the combined effects of the arc dynamics and the inherent development flow instabilities, without artificial or ad hoc artifacts. An important review and perspective on the modeling of turbulence in thermal plasma flows, including pressing challenges, current efforts, and state-of-the-art simulations, is presented by Shigeta (Ref 8).

Turbulent Thermal Plasma Flow Simulation

The computational simulation of the operation of an arc plasma torch requires the coupled solution of the set of transport and electromagnetic equations that describe the plasma flow, together with adequate constitutive relations and material properties (Ref 16). The multiphysics nature of plasma flows, their inherent nonlinearity, and large variation of material properties, together with their propensity to unstable and turbulent behavior, make their computational simulation exceedingly challenging. The modeling and simulation of turbulent plasma flows have traditionally relied on the use of models developed for other types of flows, particularly incompressible flows. Turbulence modeling is one of the most important issues in a wide range of computational fluid dynamic (CFD) applications. The main methods for the modeling and simulation of turbulent flows are divided among direct numerical simulation (DNS), Reynolds-averaged Navier–Stokes (RANS), and large eddy simulation (LES) techniques.

DNS seeks to resolve all the characteristics of the flow throughout all intervening scales, up to the smallest turbulent eddies. DNS provides the greatest accuracy but also have the greatest computational cost. The exploration via DNS of turbulent thermal plasma flows is exceedingly expensive, or even unachievable, due to the large range of scales that need to be resolved, which has prevented its use for the analysis of thermal plasma applications, particularly of plasma spraying.

RANS approaches use model equations that describe the time-averaged distributions of turbulent flow fields. RANS have a drastically reduced computational cost with respect to DNS, but at the expense of the reliance of ad hoc models and parameters. The severe modeling approximations used by RANS models limit their applicability to very-well-understood and specific flow problems. Nevertheless, their lowest computational cost makes them the outmost preferred approach for industrial flow simulations. Despite their severe modeling limitations, RANS approaches have been extensively adopted for analyses of numerous thermal plasma flows, including arc plasma torches. By far the RANS model most favored by researches has been based on the $k-\varepsilon$ (*k*-epsilon) turbulence model first developed by Launder and Spalding (Ref 17). Examples of the use of $k-\varepsilon$ models for the analysis of arc plasma torches are the work of Bauchire et al. (Ref 18), McKelliget et al. (Ref 19), Li and Chen (Ref 20), Li and Pfender (Ref 21), Huang et al. (Ref 22, 23), Yuan et al. (Ref 24, 25), and Gu et al. (Ref 26). Other RANS models applied to thermal plasmas include the Spalart–Allmaras model, which was used by Sahai et al. (Ref 27) to simulate an arc heater.

LES is a coarse-grained turbulent modeling and simulation approach that seeks to resolve the large-scale features of the flow and model the small-scale ones, which are expected to depict somewhat universal characteristics. LES provides a level of accuracy and cost somewhere in between DNS and RANS approaches, and is nowadays considered de facto standard for the exploration of turbulent flows. The vast majority of LES techniques rely on two basic assumptions, namely the suitability of spatial filters to separate scales into large and small, and the adequacy of the use of an eddy viscosity to model the redistribution of momentum from the small scales. The effects of anisotropy and nonlinearity, as well as the interaction of different physical phenomena in plasmas generally, invalidate those assumptions. Therefore, traditional LES approaches cannot, in general, be expected to provide comprehensive descriptions of turbulent plasma flows. Nevertheless, due to the absence of comprehensive LES approaches for thermal plasmas, traditional LES strategies have been adopted in thermal plasma flow simulations. For example, Colombo et al. used LES to investigate the complex unsteady 3-D turbulent flow in an inductively coupled thermal plasma torch together with its attached reaction chamber (Ref 27). Colombo et al. (Ref 26) and Ghedini and Colombo (Ref 28) employed LES to study the flow in a DC non-transferred arc plasma torch including the effect of particle injection. Furthermore, Caruyer et al. (Ref 29) used LES for the modeling of the unsteadiness and turbulence in the plasma jet from plasma torches.

A comprehensive coarse-grained plasma flow modeling and simulation method should be complete and consistent; that is, it should be free of ad hoc parameters or procedures and should be able to reproduce laminar-to-turbulent transitions naturally, and its solution has to approach that by DNS as the numerical accuracy is increased. Recently, Modirkhazeni and Trelles (Ref 30, 31) proposed the variational multiscale-*n* (VMS_n) approach for the coarse-grained simulation of general transport problems, which is particularly suited for highly nonlinear problems such as turbulent plasma flows. VMS$_n$ is based on the VMS framework (Ref 30, 32, 33), which has proven to be very versatile and robust for the solution of diverse multiphysics problems. The method uses variational scale decomposition together with a residual-based approximation of the small scales, circumventing the need for empirical parameters. The VMS$_n$ method addresses up-front the nonlinear inter-dependence between large and small scales due to the high nonlinearity in plasma flow models, distinctly exemplified in NLTE models. In this paper, the VMS and VMS$_n$ methods are evaluated for the comprehensive simulation of the flow from a DC non-transferred arc plasma spray torch.

Non-equilibrium Plasma Flow Model

Balance Equations

Fluid models, which are based on the continuum assumption and describe the evolution of the moments of the Boltzmann transport equation (Ref 34), provide appropriate descriptions of plasmas when the constituent particles experience relatively high collision frequencies, as typically found under atmospheric pressure conditions. In this paper, the plasma is considered as a nonrelativistic, nonmagnetized, quasi-neutral fluid in chemical equilibrium and thermodynamic non-equilibrium (two-temperature NLTE).

The fluid part of the plasma flow model is given by the set of conservation equations for: (1) total mass, (2) mass-averaged momentum, (3) internal energy of heavy species (i.e., neutrals and ions), and (4) internal energy of electrons. The electromagnetic fields are described by Maxwell's equations given by the (5) charge conservation and (6) magnetic induction equations. The set of fluid—electromagnetic equations describing the NLTE plasma flow—is listed in Table 1 as a single *transient–advective–diffusive–reactive* (TADR) transport system. In this table, ρ represents total mass density, $\mathbf{u}$ mass-averaged velocity, $^{\mathrm{T}}$ the transpose operator, $\boldsymbol{\delta}$ the Kronecker delta tensor, $\boldsymbol{\tau}$ the stress tensor, h_h heavy-species enthalpy, h_e electron enthalpy (from here forward, subscripts h and e stand for heavy species and electron quantities, respectively), p total pressure, T temperature, μ_0 the permeability of free space, and σ electrical conductivity. Maxwell's equations are expressed in terms of the magnetic vector potential $\mathbf{A}$ (related to the magnetic field $\mathbf{B}$ by $\mathbf{B} = \nabla \times \mathbf{A}$), and the effective electric potential ϕ_p. $\mathbf{J}_q$ is the current density and $\mathbf{E}$ the electric field; $\mathbf{J}_q \times \mathbf{B}$ describes the Lorentz force, and $\mathbf{J}_q \cdot (\mathbf{E} + \mathbf{u} \times \mathbf{B})$ Joule heating.

In the energy conservation equations, κ_h and κ_e denote the heavy species and the electron translational thermal conductivities, respectively, and κ_{hr} is the translational-reactive thermal conductivity; K_{eh} is the electron–heavy-species kinetic energy exchange coefficient; and ε_r is the effective net emission coefficient. The NLTE model is described in greater detail in Ref 1, 3, 30, 35-37.

The description of the plasma flow model as a generic TADR transport system is particularly appealing due its simplicity and the uniform handling of different physical phenomena (Ref 39). The TADR system describing the NLTE plasma flow model is expressed in so-called *residual* form by:

$$\begin{aligned}\mathcal{R}(\mathbf{Y}) &= \mathcal{L}\mathbf{Y} - \mathbf{S}_0 \\ &= \underbrace{\mathbf{A}_0\partial_t\mathbf{Y}}_{\text{transient}} + \underbrace{(\mathbf{A}_i\partial_i)\mathbf{Y}}_{\text{advective}} - \underbrace{\partial_i(\mathbf{K}_{ij}\partial_j\mathbf{Y})}_{\text{diffusive}} - \underbrace{(\mathbf{S}_1\mathbf{Y} + \mathbf{S}_0)}_{\text{reactive}} = \mathbf{0},\end{aligned} \qquad \text{(Eq 1)}$$

where $\mathbf{Y}$ is the vector of unknowns, $\mathcal{R}$ is the TADR residual, $\mathbf{A_0}$, $\mathbf{A}_i$, $\mathbf{K}_{ij}$, $\mathbf{S}_1$ are transport matrices and $\mathbf{S}_0$ a vector used to characterize each transport process, t represents time, and i and j are spatial indexes (Ref 34), and the summation of repeated indexes has been adopted. In Eq 1, $\mathcal{L}$ represents the *transport operator*, i.e., $\mathcal{L} = \mathbf{A_0}\partial_t + \mathbf{A}_i\partial_i - \partial_i(\mathbf{K}_{ij}\partial_j) - \mathbf{S_1}$. Equation 1 is complemented by the specification of initial and boundary conditions, which are omitted here for brevity of the presentation. Details of the formulation of the TADR NLTE plasma flow problem are found in Ref 33.

Up to this point, the vector of unknowns $\mathbf{Y}$ can be defined arbitrarily, as long as its components form an independent set. The set of variables to be used is the set of so-called *primitive variables* given by:

$$\mathbf{Y} = [p \quad \mathbf{u} \quad T_h \quad T_e \quad \phi_p \quad \mathbf{A}]. \qquad \text{(Eq 2)}$$

Other sets of variables could have been chosen, such as the set of conservation fluid variables $[\rho \quad \rho\mathbf{u} \quad \rho h_h \quad \rho h_e \; \phi_p \; \mathbf{A}]$. The use of primitive variables has been motivated by prior work (Ref 38) that demonstrated their advantages, especially for the unified handling of incompressible and compressible flows by a single formulation. Particularly, the fully coupled approach used here does not require the modification of the mass conservation equation as an equation for pressure p (e.g., by its modification as a Poisson equation, or by the addition of penalty terms, or artificial sound speeds).

Material Properties and Constitutive Relations

The equations in Table 2 are complemented with the definition of thermodynamic (e.g., ρ, p_h, p_e, h_h, h_e) and transport (e.g., κ_h, κ_e) properties, which add further coupling among model variables and are highly nonlinear and computationally expensive to compute, especially for NLTE models (Ref 39, 40). Thermodynamic properties link thermodynamic variables to the set of primitive variables, whereas transport properties are required for the modeling of diffusive fluxes. In typical arc plasma torches, temperatures vary from $\approx$ 300 K within the stream of working gas to $\approx$ 25 kK or higher within the arc core. Such large range implies that material properties typically vary by several orders of magnitude within a given thermal plasma flow (Ref 1, 41). In this work, argon is used as the working gas and gas environment.

The calculation of the thermodynamic properties requires knowledge of the thermochemical state of the plasma. Given the chemical equilibrium and thermodynamic non-equilibrium assumed here, the plasma state is defined in terms of the temperatures T_h and T_e, and the total pressure p. The composition is determined from them using the mass action laws, Dalton’s law of partial pressures, and the quasi-neutrality condition. Knowledge of the chemical state allows the evaluation of the thermodynamic properties ρ, h_h and h_e following standard procedures from thermodynamics.

Transport properties viscosity μ, thermal conductivities κ_{hr}, κ_e, and electrical conductivity σ for argon are computed by a table lookup procedure as function of T_e and T_h assuming $p = 1$ atm using data from Ref 42. Radiative energy transfer has a primary role in plasma flows, e.g., it is the dominant energy transport mechanism for temperatures above 30 kK (Ref 3). The direct solution of the radiative transport equation (RTE) is exceeding expensive, and consequently, diverse types of approximations are often employed. The detailed description of the radiative transport in thermal plasmas represents an enormous challenge not only because of the complex absorption spectra of the species present, but also due to the weak interaction of photons with the intervening media (inside and outside the torch). This last characteristic jeopardizes the use of models that rely on strong coupling like diffusion-like models and makes mandatory the use of more computationally expensive techniques like direct simulation Monte Carlo or directional transport methods, like ray-tracing techniques and discrete ordinates methods (DOMs).

Probably one of the best radiation transfer simulations applied to a thermal plasma flow is the work of Menart et al. (Ref 43) who used a DOM for a large set of wavelengths. Because their work was focused on analyzing radiative energy transfer, Menart et al. did not solve the radiative transport coupled to the plasma flow model. Instead, they used a pre-calculated temperature field to solve the RTE. Their approach is justified by the enormous computational cost required to solve the plasma flow together with radiative transport. An alternative approach, valid mainly when the plasma can be assumed optically thin, is the use of view factors to determine the exchange of radiative energy among the domain boundaries. Such approach has been successfully used by Lago et al. (Ref 44) for the simulation of a free-burning arc.

Table 1 Set of fluid—electromagnetic equations comprising the non-equilibrium plasma flow model; for each equation: Transient + Advective − Diffusive − Reactive = 0

Equation	Transient	Advective	Diffusive	Reactive
Conservation total mass	$\partial_t \rho$	$\mathbf{u} \cdot \nabla \rho + \rho \nabla \cdot \mathbf{u}$	0	0
Conservation momentum	$\rho \partial_t \mathbf{u}$	$\rho \mathbf{u} \cdot \nabla \mathbf{u} + \nabla p$	$\nabla \cdot \mu(\nabla \mathbf{u} + \nabla \mathbf{u}^{\mathrm{T}}) - \nabla \cdot (\frac{2}{3}\mu(\nabla \cdot \mathbf{u})\delta)$	$\mathbf{J}_q \times \mathbf{B}$
Thermal energy heavy species	$\rho \partial_t h_h$	$\rho \mathbf{u} \cdot \nabla h_h$	$\nabla \cdot (\kappa_{hr} \nabla T_h)$	$\partial_t p_h + \mathbf{u} \cdot \nabla p_h + K_{eh}(T_e - T_h) - \tau : \nabla \mathbf{u}$
Thermal energy electrons	$\rho \partial_t h_e$	$\rho \mathbf{u} \cdot \nabla h_e$	$\nabla \cdot (\kappa_e \nabla T_e)$	$\partial_t p_e + \mathbf{u} \cdot \nabla p_e - K_{eh}(T_e - T_h) - 4\pi\varepsilon_r + \mathbf{J}_q \cdot (\mathbf{E} + \mathbf{u} \times \mathbf{B}) + \frac{5k_B}{2e}\mathbf{J}_q \cdot \nabla T_e$
Conservation charge	0	0	$\nabla \cdot (\sigma \nabla \phi_p) - \nabla \cdot (\sigma \mathbf{u} \times (\nabla \times \mathbf{A}))$	0
Magnetic induction	$\mu_0 \sigma \partial_t \mathbf{A}$	$\mu_0 \sigma \nabla \phi_p - \mu_0 \sigma \mathbf{u} \times (\nabla \times \mathbf{A})$	$\nabla^2 \mathbf{A}$	$\mathbf{0}$

A detailed description of radiative transport requires solving the RTE together with proper consideration of emission and absorption processes, which make radiation modeling exceedingly involved and computationally expensive (Ref 45). Nevertheless, the form in which radiation directly interacts with the plasma flow (i.e., as a *reactive* term) suggests that detailed description of radiation transfer is not essential and that direct approximations of the $\nabla \cdot \mathbf{q}_r$ term could be used, where $\mathbf{q}_r$ is the radiative heat flux. In this regard, the most common approximation in thermal plasma modeling is the use of the *effective net emission* approximation $\nabla \cdot \mathbf{q}_r \neq 4\pi\varepsilon_r$ (Ref 46-48), where the coefficient ε_r is a function of the state of thermodynamic state of the plasma and a given *effective absorption* radius. The latter represents the radius of a sphere in which the emitted radiation can be re-absorbed; outside of this sphere, the emitted radiation leaves without further interaction with the plasma. (Hence, the optically thin approximation implies that this radius is zero). The net emission approach is particularly appealing for plasma flow simulation because ε_r can be treated as any other material property. For the argon plasma studied in this paper, the net emission coefficient for argon was computed as $\varepsilon_r = \varepsilon_r(T_e)$ using a lookup table procedure based on the data reported in Ref 46 assuming optically thin plasma (i.e., absorption radius equal to zero), which can overestimate radiative energy losses and hence significantly reduce the temperature within the core of the plasma, but should have a minor effect within the jet due to its significantly lower temperature.

The kinetic energy exchange coefficient K_{eh} is computed by:

$$K_{eh} = \sum_{s \neq e} \frac{3}{2} k_{\mathrm{B}} \frac{2 m_s m_e}{(m_s + m_e)^2} \nu_{es}. \tag{Eq 3}$$

where k_{B} is Boltzmann's constant, m_s the mass of species, m_e the electron mass, and ν_{es} the collision frequency between electrons and species s given by: $\nu_{es} = \bar{u}_e n_e \sigma_{es}$, where $\bar{u}_e = (8 k_{\mathrm{B}} T_e / \pi m_e)^{\frac{1}{2}}$ is the thermal speed of electrons and σ_{es} is the collision cross section between electrons and species s computed following Ref 33. The detailed evaluation of material properties for the NLTE plasma flow model is described in Ref 33, 41, and 49.

The use of primitive variables makes necessary the evaluation of the derivatives of thermodynamic properties (ρ, ρh_h, ρh_e) with respect to the state variables (p, T_h, T_e) for the evaluation of the transport matrices ($\mathbf{A_0}$, $\mathbf{A}_i$, etc.). These terms constitute additional thermodynamic properties that link conservation and primitive variables, which are evaluated using discrete differentiation, e.g.,

$$\frac{\partial \rho}{\partial p}(p, T_h, T_e) \approx \frac{\rho(p + \delta_p, T_h, T_e) - \rho(p, T_h, T_e)}{\delta_p}, \tag{Eq 4}$$

where $\rho(p,\ T_h,\ T_e)$ explicitly indicates the functional dependence of ρ on p, T_h, T_e, and δ_p is a small discrete differential. The inclusion of such terms within the transport matrices (i.e., instead as source terms) has proven to aid in the numerical convergence of the NLTE model (Ref 32).

Numerical Model

Variational Multiscale-*n* Formulation

The complex coupling among model variables, together with the high nonlinearity and large variation of material properties, makes numerical counterparts of the NLTE plasma flow model very stiff. Numerical stiffness is a somewhat broad concept related to largely disparate temporal and/or spatial characteristics of the solution and is more directly related to the *multiscale* nature of the problem. The numerical solution of the NLTE plasma flow model given by Eq 1 is based on variational multiscale (VMS) framework (Ref 33, 34). VMS methods effectively address the challenges associated with multiscale problems, which makes them ideal for the solution of transport problems. Particularly, the VMS$_n$ method constitutes an extension of the classical VMS approach to directly account for the intricate nonlinear coupling among large and small scales, as particularly found in turbulent flows.

VMS methods use the variational form of Eq 1, namely

$$(\mathbf{W}, \mathcal{R}(\mathbf{Y}))_\Omega = \mathbf{0}, \tag{Eq 5}$$

where $(\cdot,\cdot)_\Omega$ indicates the bilinear operator $(f,g)_\Omega = \int_\Omega f \cdot g \mathrm{d}\Omega$, and $\mathbf{W}$ is the test function (belonging to an appropriate functional space consistent with $\mathbf{Y}$ and the definition of the problem in Eq 1, see Ref 33). VMS methods have two main components: scale decomposition and approximation of the small scales. Let the solution field $\mathbf{Y}$ be decomposed into a large-scale component $\bar{\mathbf{Y}}$ (grid scale, described by the numerical discretization) and a small-scale component $\mathbf{Y}'$ (sub-grid, unresolved by the discretization), i.e., $\mathbf{Y} = \bar{\mathbf{Y}} + \mathbf{Y}'$. This decomposition implies decomposition of the continuous space $\mathcal{V}$ ($\mathcal{V} = \bar{\mathcal{V}} + \mathcal{V}'$) where $\mathbf{Y}$ belongs. The space $\bar{\mathcal{V}}$ is formally defined by the use of a projector operator (Ref 50, 51). The transport matrix in most fluid models is nonlinear, i.e., $\mathcal{L}$=$\mathcal{L}(\mathbf{Y})$; moreover, for the NLTE plasma flow model, this nonlinearity is non-separable; that is, the functional dependency of the transport matrices on $\mathbf{Y}$ cannot be explicitly separated into the large- and small-scale terms (e.g., $\mathbf{A}_i(\mathbf{p}+\mathbf{q}) \neq \mathbf{A}_i(\mathbf{p}) + \mathbf{A}_i(\mathbf{q})$, and therefore, $\mathbf{A}_i \neq \bar{\mathbf{A}}_i + \mathbf{A}'_i$). The VMS$_n$ method is motivated by the need to address such complex nonlinearity up-front (i.e.,

$\mathcal{L} = \mathcal{L}(\bar{\mathbf{Y}} + \mathbf{Y}'))$, as required for the comprehensive description of plasma turbulence. (In contrast, traditional VMS methods assume $\mathcal{L} = \mathcal{L}(\bar{\mathbf{Y}})$, which is a reasonable approximation for problems in which the large and small scales are not tightly coupled.)

Using the scale decomposition, the weak form of the transport problem leads to two separate problems: one for the large scales and another one for the small scales, i.e.,

$$(\bar{\mathbf{W}}, \mathcal{L}\bar{\mathbf{Y}} - \bar{\mathbf{S}}_0)_\Omega + (\mathcal{L}^* \bar{\mathbf{W}}, \mathbf{Y}')_\Omega \\ = \mathbf{0} \text{ and } (\mathbf{W}', \mathcal{L}\bar{\mathbf{Y}} - \bar{\mathbf{S}}_0)_\Omega + (\mathcal{L}^* \mathbf{W}', \mathbf{Y}')_\Omega = \mathbf{0}. \qquad \text{(Eq 6)}$$

where * is the adjoint operator (Ref 52). To obtain a tractable and computationally efficient model, the VMS$_n$ method relies on approximately solving the equation for the small scales (right side of Eq 6) locally by approximating $\mathcal{L}^{-1}$ with an algebraic operator τ, the so-called intrinsic time scales matrix (Ref 33), i.e., $\tau \approx \mathcal{L}^{-1}$. Using this approximation, the solution of small-scale problem is given by:

$$\mathbf{Y}' = -\tau(\mathcal{L}\bar{\mathbf{Y}} - \bar{\mathbf{S}}_0), \qquad \text{(Eq 7)}$$

where $\tau = \tau(\bar{\mathbf{Y}} + \mathbf{Y}')$ and $\mathcal{L} = \mathcal{L}(\bar{\mathbf{Y}} + \mathbf{Y}')$. There are numerous approaches to obtain an expression for τ; the present work utilizes the *diagonal approximation* of the transport matrices (Ref 32, 33). Equation 7 represents a nonlinear system for $\mathbf{Y}'$ that depends on the large scales $\bar{\mathbf{Y}}$. Classical VMS formulations have relied on Eq 7 and the assumptions $\tau \approx \tau(\bar{\mathbf{Y}})$ and $\mathcal{L} \approx \mathcal{L}(\bar{\mathbf{Y}})$ (i.e., the contributions due to the small scales are neglected), which makes the small-scale problem linear on $\mathbf{Y}'$. In contrast, the VMS$_n$ formulation addresses the full nonlinear problem given by Eq 7.

The final VMS$_n$ formulation used in the present work consists of the following two problems:

$$\bar{\mathbf{R}}(\bar{\mathbf{Y}}; \mathbf{Y}') \\ = \underbrace{(\bar{\mathbf{W}}, (\mathbf{A}_0\partial_t + \mathbf{A}_i\partial_i - \mathbf{S}_1)\bar{\mathbf{Y}} - \bar{\mathbf{S}}_0)_\Omega + (\partial_i\bar{\mathbf{W}}, \mathbf{K}_{ij}\partial_j\bar{\mathbf{Y}})_\Omega - (\bar{\mathbf{W}}, \mathbf{K}_{ij}\partial_j\bar{\mathbf{Y}})_\Gamma}_{\text{large}-\text{scales}} \\ + \underbrace{((\mathbf{A}_0^{\mathrm{T}}\partial_t + \mathbf{A}_i^{\mathrm{T}}\partial_i + \partial_i(\mathbf{K}_{ij}^{\mathrm{T}}\partial_j) + \mathbf{S}_1^{\mathrm{T}})\bar{\mathbf{W}}, \mathbf{Y}')_{\Omega'}}_{\text{small}-\text{scales}} + \underbrace{(\partial_i\bar{\mathbf{W}}, \mathbf{K}_{ij}^{DC}\partial_j\bar{\mathbf{Y}})_{\Omega'}}_{\text{discontinuitycapturing}} = \mathbf{0} \qquad \text{(Eq 8)}$$

and

$$\mathbf{R}'(\mathbf{Y}'; \bar{\mathbf{Y}}) = \mathbf{Y}' + \tau(\mathcal{L}\bar{\mathbf{Y}} - \bar{\mathbf{S}}_0) = \mathbf{0}, \qquad \text{(Eq 9)}$$

where the notation $f(a;b)$ (referring to $\bar{\mathbf{R}}(\bar{\mathbf{Y}}; \mathbf{Y}')$ and $\mathbf{R}'(\mathbf{Y}'; \bar{\mathbf{Y}})$) indicates that the function f has as argument a and depends parametrically on b; $\bar{\mathbf{R}}$ represents the residual of the large-scale problem and $\mathbf{R}'$ the residual form of the small-scale problem. Equation 8 and 9 are both nonlinear on $\bar{\mathbf{Y}}$ and $\mathbf{Y}'$, given that the transport matrices depend nonlinearly on $\mathbf{Y}$. The last term in Eq 8 is the *discontinuity-capturing* operator, used to minimize the occurrence of spurious oscillations near unresolved high-gradient regions, as well to increase the robustness of the solution approach. The anisotropic version of the *discontinuity-capturing diffusivity matrix* $\mathbf{K}_{ij}^{DC}$ is used in the present work (Ref 32, 33). The model given by Eq 8 and 9 is similar to most VMS formulations (e.g., Ref 33, 38, 53-55). The main distinction of the VMS$_n$ method is its formulation for highly multiscale nonlinear TADR problems, as required for the description of turbulence in the NLTE plasma flow model, as well as its solution of the small-scale model, described next.

Solution of the Small-Scale Problem

The small-scale model in Eq 9 constitutes a nonlinear algebraic problem for $\mathbf{Y}'$ (given that $\tau = \tau(\bar{\mathbf{Y}} + \mathbf{Y}')$ and $\mathcal{L} = \mathcal{L}(\bar{\mathbf{Y}} + \mathbf{Y}')$), which can be solved by different methods. Newton-like methods, in order to evaluate $\partial\mathcal{L}/\partial\mathbf{Y}'$, require additional evaluations of the transport matrices of the form $\mathbf{A}(\mathbf{Y}' + \delta\mathbf{Y}')$, where $\delta\mathbf{Y}'$ is a small variation, or of their derivative, e.g., $\partial\mathbf{A}/\partial\mathbf{Y}'$; both of which can be very expensive to compute in highly nonlinear problems such as in the NLTE plasma flow model (Ref 33). The VMS$_n$ formulation uses a fixed-point (Picard) iteration due to its simplicity and limited cost. Given a prior approximation n of $\mathbf{Y}'$, a new one, $n + 1$, is obtained using the recurrence relations:

$$\begin{aligned} \mathcal{L}^{n+1} &= \mathcal{L}(\bar{\mathbf{Y}} + \mathbf{Y}'^n), \\ \tau^{n+1} &= \tau(\bar{\mathbf{Y}} + \mathbf{Y}'^n), \\ \mathbf{Y}'^{n+1} &= -\tau^{n+1}(\mathcal{L}^{n+1}\bar{\mathbf{Y}} - \bar{\mathbf{S}}_0), \end{aligned} \qquad \text{(Eq 10)}$$

where the superscript n indicates the iteration counter, and $\bar{\mathbf{Y}}$ and $\bar{\mathbf{S}}_0$ are treated as parameters.

The VMS$_n$ formulation has been implemented in the TPORT (TransPORT) solver (Ref 56). TPORT is designed for solving general systems of TADR equations of the form of Eq 1. TPORT is written in C++ and performs parallel processing in shared-memory architectures using Open Multi-Processing (OpenMP) and in distributed-memory systems using PETSc. In TPORT, the solution to Eq 8 and 9 is perused by using a version of a second-order generalized-alpha predictor multicorrector time-stepper method developed by Jansen and collaborators (Ref 57) together with the globalized inexact Newton–Krylov nonlinear solver approach of Eisenstat and Walker (Ref 58). The TPORT code has been extensively used for the simulation of scalar transport, incompressible and compressible flow problems, radiative transport, and equilibrium (LTE) and non-equilibrium (NLTE) plasma flows (e.g., see Ref 30-33, 41 and references therein).

Validation of VMS$_n$ Method with Turbulent Incompressible Free Jet

Turbulent Free Jet

The simulation of an incompressible turbulent jet is investigated to evaluate the VMS$_n$ method and as a preliminary step to the simulation of the non-equilibrium turbulent plasma flow in an arc plasma torch. The problem setup, domain boundaries, and underlying spatial discretization are presented in Fig. 2(a). In Fig. 2(a), D indicates the outlet jet diameter, and W and L the width and length of the discharge domain, respectively. The free jet problem setup can be contrasted against that for the non-transferred arc torch, as shown in Fig. 2(b).

The boundary conditions are defined as follows: for the *wall* boundary: $\partial_n p = 0$ and $\mathbf{u} = \mathbf{0}$; for *inlet*: $\partial_n p = 0$ and $\mathbf{u} = [0\ 0\ U_{\text{in}}]$; and for *outlet*: $p = p_{\text{atm}}$ and $\partial_n \mathbf{u} = 0$. U_{in} is the average velocity at the inlet and $p_{\text{atm}} = 1.01325$ [10^5 Pa] represents atmospheric pressure. The working fluid is argon. In order to investigate the capabilities of the VMS$_n$ method under different levels of turbulence, two values of Reynolds number $Re = \rho U_{in} D/\mu$ are considered, i.e., $Re = 5142$ and $Re = 20{,}000$. Both values of Re have been extensively studied in the literature, and according to Ref 59, 60, both Re lead to turbulent jets. For each Re, simulations are performed using VMS$_n$, VMS, and the dynamic Smagorinsky [LES, presented by Germano et al. (Ref 61) and Lilly (Ref 62)] methods. The dynamic Smagorinsky method is often considered the workhorse for turbulent incompressible flow simulations; its use here is intended to provide a benchmark against the VMS and VMS$_n$ results. It is to be noted that the dynamic Smagorinsky simulations here were run using the commercial software ANSYS Fluent (Ref 63) (in contrast to TPORT for the VMS and VMS$_n$ results).

All the simulations in this work used spatial discretizations based on trilinear basis functions (i.e., 6-node hexahedra). For simulations with $Re = 5142$, the computational grid consists of $\sim$ 230 k nodes and $\sim$ 235 k elements with $D = 0.0088$ m, $L = 0.3$ m, and $W = 0.088$ m, whereas for $Re = 20{,}000$, the grid is made of $\sim$ 245 k nodes and $\sim$ 251 k elements, $D = 0.0088$ m, $L = 0.35$ m, and $W = 0.08$ m. Both grids are structured with a non-uniform distribution of elements. In order to reduce the computational time to observe the evolution of the flow into a turbulent state, the inflow velocity profile is modified with random spatial perturbations with a standard deviation of 5% of the magnitude of the average inlet velocity ($5\% U_{\text{in}}$), which was constant in time for the VMS and VMS$_n$ simulations, and time dependent for the dynamic Smagorinsky simulations (default setting for LES approaches in Fluent).

The instantaneous and time-averaged results using the three methods for $Re = 5142$ and $Re = 20{,}000$ are summarized in Fig. 3. The instantaneous velocity distributions depict the turbulent nature of the flow, whereas the time-averaged ones show the overall characteristics of the flow, such as the overall decay of the jet's average velocity, which gives an indication of the location where turbulent features become significant. In this regard, the white arrows in the time-averaged plots in Fig. 3 refer to the location where the velocity magnitude along the jet's axis reaches 80% of U_{in}. This location can be considered as the onset of dominant turbulent behavior. Due to the transient nature of turbulence, the jet simulations are associated with diverse oscillations and instabilities, which make it difficult to judge when the convergence to a statistically steady distribution is achieved. The time-averaged results in Fig. 3 are obtained by averaging simulation data during at least 20,000 times the characteristic time scale for the small eddies defined as $\tau_s = Re^{-1/2} D/U_{\text{in}}$ (based on Kolmogorov's theory (Ref 64)). Each simulation used the same and constant time step Δt such that $\Delta t < \tau_s$.

The instantaneous results in Fig. 3 show that for both Re numbers, the jet appears to be significantly more laminar for the VMS method compared to those for the dynamic Smagorinsky and VMS$_n$ methods. The amount of turbulent dissipation produced by each method is better contrasted by the time-averaged results of Fig. 3, which indicates that the locations where the axial velocity decays to 80% of U_{in} are significantly lower for the VMS$_n$ method than for VMS, for both $Re = 5142$ and $Re = 20{,}000$; the results for VMS$_n$ are very similar to those for the dynamic Smagorinsky. Therefore, for the same computational domain and Re, VMS$_n$ is more capable of capturing the turbulent characteristics of the flow than VMS, and its accuracy is comparable to that by the dynamic Smagorinsky method. As expected, more turbulent behavior in the flow is observed for the larger values of Re. Figure 3 also shows that the difference between the locations in which the axial velocity decays to $80\% U_{\text{in}}$ for the VMS and VMS$_n$ methods is approximately conserved for different values of Re. It has to be mentioned that the results are expected to be dependent on the resolution of the mesh, e.g., the results using VMS should approach those by VMS$_n$ as the computational grid is refined.

In all the simulations presented here, the inlet velocity is spatially perturbed with standard deviation of 5% of the average inlet velocity. Such perturbation of the inflow is depicted in Fig. 4(a). For a flow that evolves turbulence, the resulting flow characteristics are expected to be

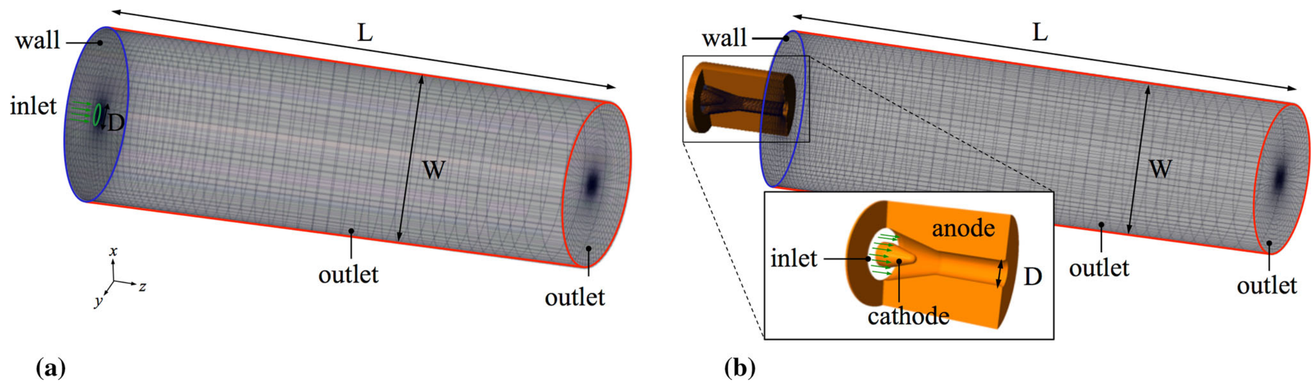

Fig. 2 Model geometry, boundaries, and computational mesh formed by hexahedral trilinear elements for (a) incompressible turbulent free jet and (b) flow from a non-transferred arc plasma torch

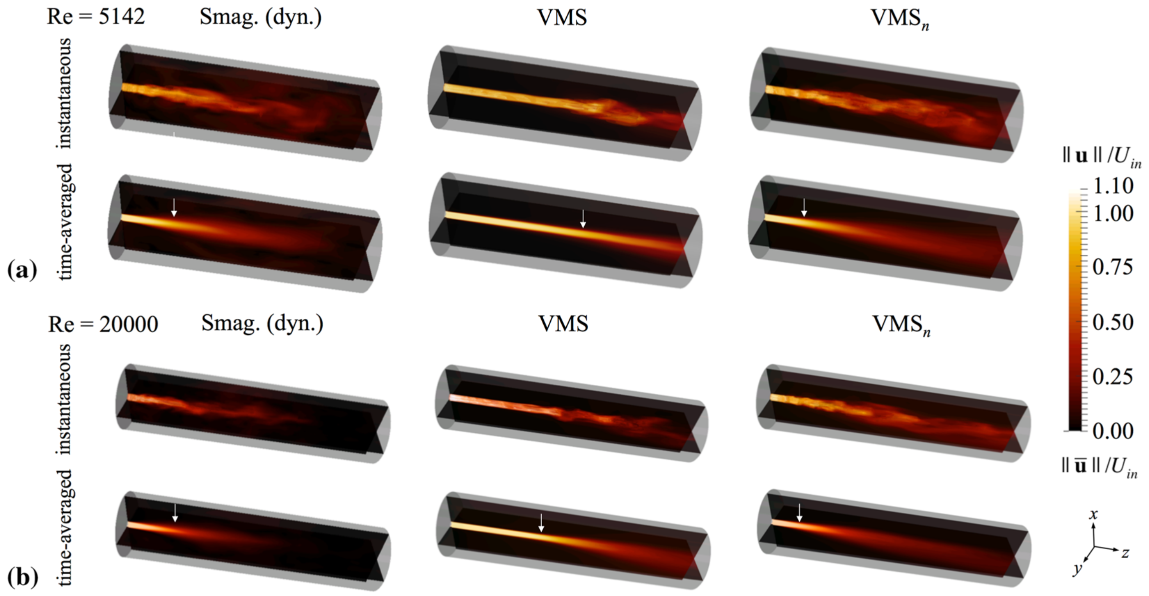

Fig. 3 Incompressible turbulent jet simulations: instantaneous and time-averaged normalized velocity magnitudes for (a) *Re* = 5142 and (b) *Re* = 20,000 using the dynamic Smagorinsky, VMS, and VMS$_n$ methods. The arrows indicate the location where the velocity has decayed to 80% of the inlet value

independent of the type and magnitude of the seeded perturbations (as long as they are appropriately small). These instabilities typically decay if the flow is laminar or if the numerical approach is not suitable for turbulent flow simulations (e.g., if the method produces excessive numerical dissipation). In order to show such behavior, two simulations using the VMS and VMS$_n$ methods for the incompressible free jet with *Re* = 500 have been performed. The same geometry and computational domain as those that were used for the set of simulations for *Re* = 5142 are utilized, and the corresponding results are presented in Fig. 4(b). The results show that although the inlet velocity is perturbed (i.e., Fig. 4a), the instantaneous velocity distributions are laminar for both the VMS and VMS$_n$ methods. Therefore, the fluctuations considered at inflow for velocity distribution did not influence the laminar behavior of the jet.

Incompressible and Compressible Gas Flow in a Non-transferred Torch

Incompressible Gas Flow in a Non-transferred Torch

As a preliminary step to the VMS$_n$ simulation of the NLTE plasma flow in an arc plasma torch, the incompressible flow through a non-transferred arc plasma torch is investigated using both VMS and VMS$_n$ approaches. The domain geometry and boundaries that are shown in

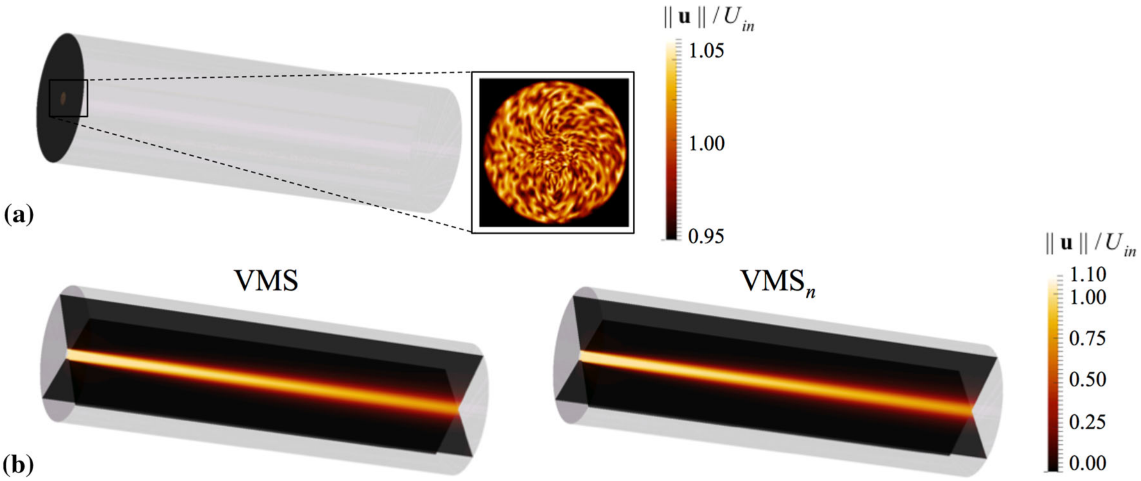

Fig. 4 Inflow velocity perturbations and turbulence development for the incompressible jet for $Re = 500$: (a) inlet velocity profile perturbed by 5% of the average velocity and (b) instantaneous velocity distribution using the VMS and VMS$_n$ methods

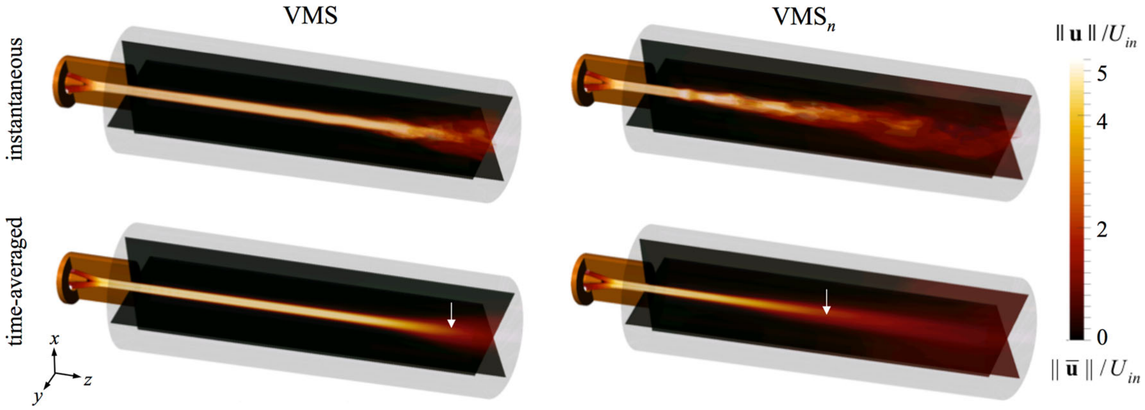

Fig. 5 Incompressible flow from an arc plasma torch for $Re_{\text{jet}} = 5142$: instantaneous and time-averaged normalized velocity magnitudes using the VMS and VMS$_n$ methods. The arrows indicate the start of dominant turbulent characteristics in the flow

Fig. 2(b) have $D = 0.0088$ m (diameter of the torch outlet), $L = 0.3$ m (length of the outflow domain), and $W = 0.08$ m (width of the outflow domain), and have been discretized using ~ 386 k nodes and ~ 375 k trilinear hexahedral elements. Simulations used argon as the working fluid with boundary conditions defined by: *wall*, *cathode*, and *anode* boundaries: $\partial_n p = 0$ and $\mathbf{u} = \mathbf{0}$; *inlet* boundary: $\partial_n p = 0$ and $\mathbf{u} = [0\ 0\ U_{\text{in}}]$; and *outlet* boundary: $p = p_{\text{atm}}$ and $\partial_n \mathbf{u} = 0$. The average velocity, U_{in}, is defined such that that if the Re number at the exit of the torch was computed based on the average velocity of the jet, the value of Re equals 5142.

Representative simulation results are shown in Fig. 5. Similarly as for the incompressible free jet, the VMS$_n$ results appear more turbulent than those using VMS. Consequently, the VMS$_n$ formulation is more capable of resolving the small structures in the flow than the VMS one. The success of VMS$_n$ in modeling the turbulent incompressible flow from a non-transferred arc plasma torch establishes expectations to achieve higher accuracy using VMS$_n$ approach for the turbulent plasma simulation.

Compressible Gas Flow in a Non-transferred Torch

The compressible flow simulation of the flow from a non-transferred torch using a computational domain discretized by ~ 351 k trilinear hexahedral elements and ~ 362 k nodes with $D = 0.0088$ m, $L = 0.25$ m, and $W = 0.08$ m using argon as the working gas is considered next. The mesh is finer near the cathode tip and stretched toward solid boundaries to better resolve boundary layers. Based on the obtained locations for the start of turbulence in the incompressible flow cases, for the compressible and plasma flow simulations, the length of the domain (L) was

Table 2 Set of boundary conditions for the non-transferred arc plasma torch simulation

Boundary	Variable					
	p	$\mathbf{u}$	T_h	T_e	ϕ_p	$\mathbf{A}$
Cathode	$\partial_n p = 0$	$\mathbf{u} = \mathbf{0}$	$T_h = T_{\text{cath}}(z)$	$\partial_n T_e = 0$	$-\sigma\partial_n\ \phi_p = \mathbf{J}_{q\text{cath}}(z)$	$\partial_n \mathbf{A} = \mathbf{0}$
Anode	$\partial_n p = 0$	$\mathbf{u} = \mathbf{0}$	$-\kappa_h \partial_n T_h = h_w(T_h - T_w)$	$\partial_n T_e = 0$	$\phi_p = 0$	$\partial_n \mathbf{A} = \mathbf{0}$
Inlet	$\partial_n p = 0$	$\mathbf{u} = \mathbf{u}_{\text{in}}$	$T_h = T_{\text{in}}$	$T_e = T_{\text{in}}$	$\partial_n\ \phi_p = 0$	$\mathbf{A} = \mathbf{0}$
Outlet	$p = p_{\text{out}}$	$\partial_n \mathbf{u} = \mathbf{0}$	$\partial_n T_h = 0$	$\partial_n T_e = 0$	$\phi_p = 0$	$\partial_n \mathbf{A} = \mathbf{0}$
Wall	$\partial_n p = 0$	$\mathbf{u} = \mathbf{0}$	$T_h = T_w$	$\partial_n T_{\text{e}} = 0$	$\partial_n\ \phi_p = 0$	$\partial_n \mathbf{A} = \mathbf{0}$

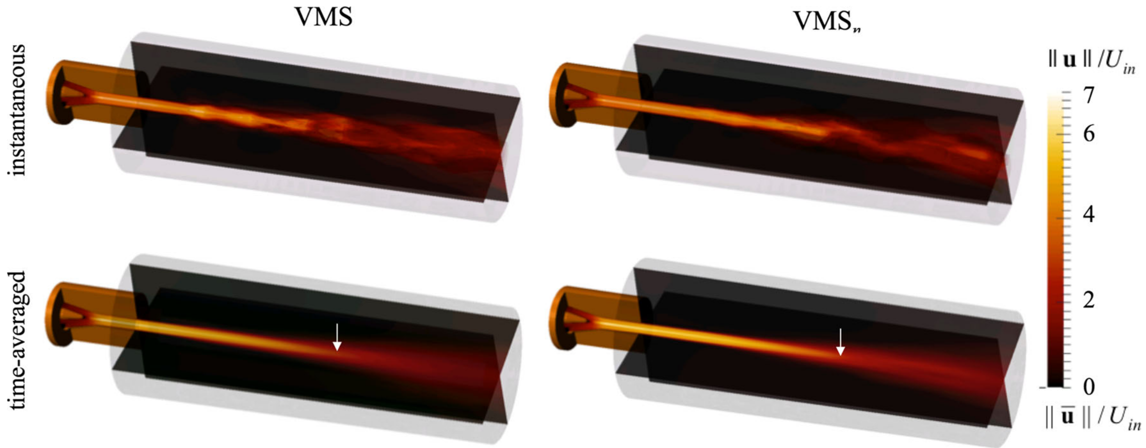
VMS
VMS$_n$
instantaneous
time-averaged
$\| \mathbf{u} \| / U_{in}$
7
6
4
2
0
$\| \bar{\mathbf{u}} \| / U_{in}$

Fig. 6 Compressible flow from an arc plasma torch: instantaneous and time-averaged normalized velocity magnitudes for $Q_{\text{in}} = 40$ slpm ($Re_{\text{in}} = 1857$ and $Re_{\text{jet}} = 183$) using VMS and VMS$_n$ methods. The arrows indicate the location where the maximum velocity decays by $\sim$ 60% (indicative of the start of dominant turbulent behavior)

shortened. Nevertheless, the number of elements is approximately conserved; that is, the mesh is finer than those used in the simulations in Fig. 5.

The set of boundary conditions utilized for the compressible flow simulations is given in Table 2 as a subset of the conditions used for the NLTE plasma flow simulations (i.e., only one temperature is used, and there are no conditions imposed for the electric and magnetic potentials). A uniform velocity profile is imposed at the torch inlet such to describe a volumetric inflow Q_{in} of 40 slpm which corresponds to a Re number of $Re_{\text{in}} = 1857$ at the torch inlet. If the Re number at the exit of the torch was computed based on the average velocity of the exiting jet, the value of Re would equal 183. (The velocity distribution at the torch exit is not uniform.) Also, a hot cathode surface is included in the compressible simulations in order to maintain consistency with the subsequent NLTE plasma flow simulations [where the relatively high cathode temperatures describe the heating of the tungsten cathode for thermionic emission (Ref 1)].

In order to compare the performance of the VMS and VMS$_n$ methods, instantaneous and time-averaged normalized velocity and temperature distributions are shown in Fig. 6 and 7. These figures show that for the same computational configurations, there is no significant difference between the time-averaged results of simulations with VMS and VMS$_n$. The similarity in the velocity distributions obtained using both methods is indicated by the relatively similar location of the white arrows in Fig. 6 (location in which the average axial jet velocity reaches 40% of the maximum velocity). Hence, the onset of turbulent behavior predicted by the VMS and VMS$_n$ methods is similar, in marked contrast to the incompressible flow results in Fig. 5. The most recognizable difference between the VMS and VMS$_n$ results is observed in regions close to the end of the domain as it is demonstrated in Fig. 7(b). (In this figure, the temperature distributions in part (a) are re-colored considering the range of $0.5 < T < 0.55$ kK for temperature.) Inside the torch, the behavior of the two different approaches, in terms of velocity and temperature distributions, is very similar to each other.

The similarity in the location of the onset of turbulent behavior in the compressible flow results is largely due to the increased temperature of the flow. The higher-temperature distributions are due to the temperature boundary condition over the cathode (Table 2). Higher temperature affects the value of density and viscosity of the fluid, which can affect the value of Re of the exiting jet from the torch.

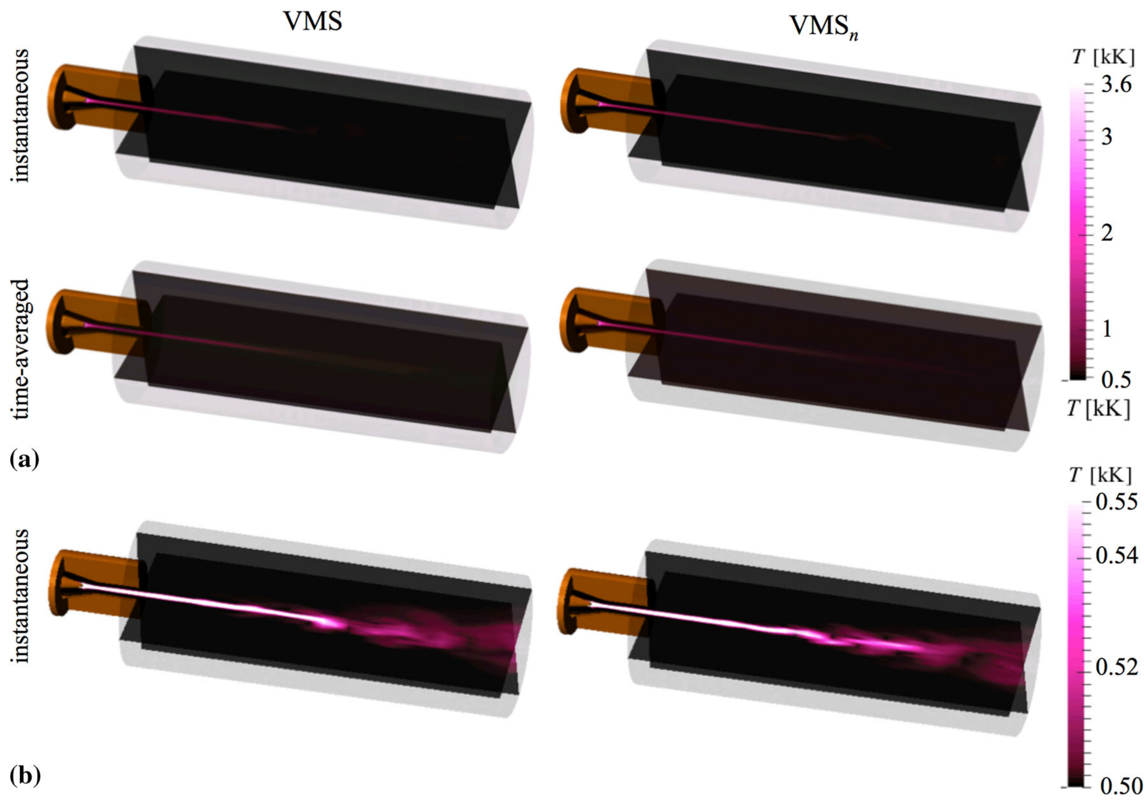

Fig. 7 Compressible flow from an arc plasma torch: temperature distributions for Q_{in} = 40 slpm (Re_{in} = 1857 and Re_{jet} = 183) using VMS and VMS$_n$ methods: (a) instantaneous and time-averaged temperature distributions for the whole range of temperature associated with the problem and (b) instantaneous temperature distributions demonstrated in a range of $0.50 < T < 0.55$ kK

Although the results in Fig. 5 and 6 correspond to simulations for different Re, the representation of non-dimensional velocity distributions makes it possible to compare them. Contrasting the location of the arrows using the VMS$_n$ method in Fig. 5 and 6, it is concluded that the onset of turbulence for incompressible and compressible simulation is approximately the same (i.e., $L/D \sim 13$). This observation has important implications in the interpretation of the NLTE plasma flow results, as presented next.

Turbulent Non-equilibrium Flow from a Non-transferred Arc Plasma Torch

Problem Setup

Simulation of the NLTE plasma flow in a non-transferred arc torch is carried out using the geometry and domain shown in Fig. 2(b) and the set of boundary conditions in Table 2. The computational domain is the same as the one used for the compressible flow simulations.

In Table 2, $\partial_n \equiv \mathbf{n}\cdot\nabla$, where $\mathbf{n}$ is the outer normal to the surface, denotes the derivative in the direction of the outer normal to the surface, p_{out} is set equal to the atmospheric pressure (1.01325×10^5 Pa). The volumetric flow rate Q_{in}, similarly as for the compressible flow simulations, is set to 40 slpm using straight (no swirl) gas injection. Hence, the inflow velocity profile, assumed as uniform, is such that $Q_{\mathrm{in}} = \int_{S_{\mathrm{inlet}}} \mathbf{u}_{\mathrm{in}} \mathrm{d}S = U_{\mathrm{in}} S_{\mathrm{inlet}} \hat{z}$, where S_{inlet} is the inlet surface and $\hat{z}$ the unit vector along the torch axis.

T_{cath} is the temperature profile over the cathode surface described by:

$$T_{\mathrm{cath}} = T_{\mathrm{crod}} + (T_{\mathrm{ctip}} - T_{\mathrm{crod}})\exp\left(-(z/L_{\mathrm{cath}})^2\right), \qquad \text{(Eq 11)}$$

where T_{crod} and T_{ctip} are the temperatures of the cathode rod and tip equal to 500 and 3600 K, respectively, and L_{cath} is a characteristic length of the temperature profile equal to 1.5 mm; $h_w = 10^5$ Wm^{-2} K^{-1} is the convective heat transfer coefficient and T_w = 500 K a reference temperature for the water cooling of the anode; T_{in} = 500 K is the imposed inflow temperature; and $J_{q\mathrm{cath}}$ the current density:

$$J_{q\mathrm{cath}} = J_{q\max} \exp\left(-(r/r_{\mathrm{cath}})^{n_{\mathrm{cath}}}\right), \qquad \text{(Eq 12)}$$

where $J_{q\max} = 2.25 \times 10^8$ A m^{-2}, $r = (x^2 + y^2)^{1/2}$ is the radial coordinate, and r_{cath} = 0.4236 mm and n_{cath} = 4 are parameters that control the shape of the current density profile, which satisfy the imposition of the total current to the system, i.e., $I_{\mathrm{tot}} = \int_{S_{\mathrm{cath}}} J_{q\mathrm{cath}} \mathrm{d}S$, where S_{cath} is the cathode surface.

Simulation Results

Turbulent non-equilibrium plasma flow simulations of the DC non-transferred arc plasma torch are performed using both the VMS and VMS$_n$ approaches. Representative simulation results for the torch operating with argon, $Q_{\mathrm{in}} = 40$ slpm and $I_{\mathrm{tot}} = 400$ A using the VMS$_n$ method, are presented in Fig. 8. The figure shows the instantaneous distributions of heavy species temperature T_h and electron temperature T_e, thermodynamic non-equilibrium parameter $\theta = T_e/T_h$, velocity magnitude ||**u**||, effective electric potential ϕ_p, and magnitude of the magnetic vector potential ||**A**||. The results show the formation of the cathode jet due to electromagnetic pumping and intense heating near the cathode. The maximum temperatures of the heavy species and electrons are above 25 kK, and the value of θ is close to one within the core of the plasma (i.e., thermodynamic equilibrium is achieved) and increases significantly near the cooling walls. Such behavior cannot be described by LTE models and emphasizes the importance of the use of NLTE models. According to Fig. 8, thermodynamic non-equilibrium is dominant in the regions where the cold processing gas flow interacts with the plasma. The higher θ regions near the cathode tip and immediately upstream of the anode column indicate that non-equilibrium increases as the strength of the plasma–gas flow interaction increases. Whereas the distributions of both, T_h and T_e, show the large-scale undulating characteristics of the jet, the distribution of T_h displays some fine-scale features not observed in the T_e distribution. The distribution of T_e is more diffusive, as expected due to by the higher thermal conductivity of electrons than that of the heavy species (Ref 42, 65).

In DC arc plasma torches, the working gas is typically at ambient temperature when it enters the torch. The temperature of the gas, as it interacts with the arc, increases by a rate of order 10^4 K mm^{-1}. This rapid heating causes the sudden expansion of the gas and consequently its rapid acceleration. The velocity of the gas across the torch often varies by over 2 orders of magnitude (e.g., from $O(10)$ to $O(1000)$ ms^{-1}). Such trend can be observed in the simulation results in Fig. 8. The large gas acceleration and shear velocity and temperature gradients inside the torch, together with the electromagnetic forcing, cause the flow to become unstable and turbulent. According to Fig. 8, turbulence is further enhanced when the plasma flow leaves the torch and interacts with the cold environment, which is consistent with experimental observations. Furthermore, the distribution of ϕ_p shows a maximum voltage drop of 35 V. The distribution of magnetic vector potential shows that the magnetic field is self-induced, and the approximately linear gradient of ||**A**|| along the z-axis indicates that the magnetic field should act as constricting the arc radially. The distributions of ϕ_p and ||**A**|| in Fig. 8 show

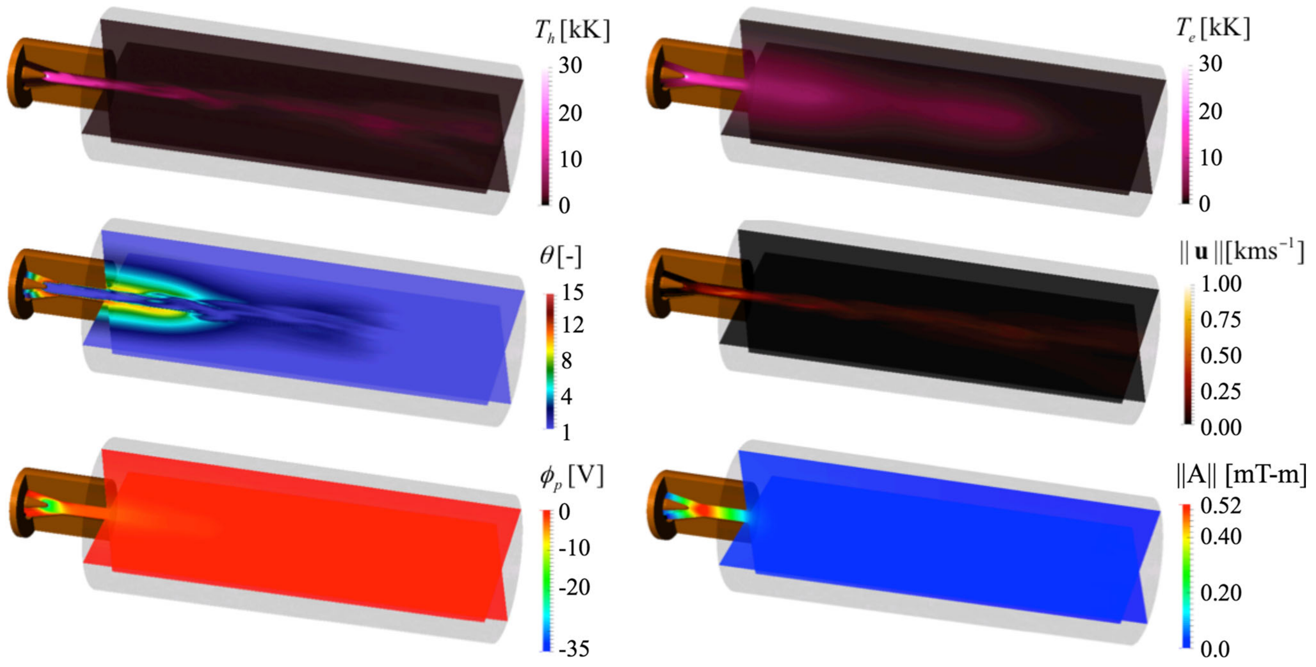

Fig. 8 Solution fields for the non-transferred arc plasma torch using VMS$_n$ method: heavy-species temperature T_h, electron temperature T_e, thermodynamic non-equilibrium parameter $\theta = T_e/T_h$, velocity vector magnitude ||**u**||, effective electric potential ϕ_p, and magnitude of magnetic vector potential ||**A**||. Conditions: gas: Ar; flow rate: 40 slpm; total current: 400 A

marked resemblance with computational observations of the dynamics of plasma jets such as those reported in Ref 33.

The balance between the Lorentz force and the drag caused by the cold working gas is the main factor determining the dynamics of the arc inside DC non-transferred torches. The ratio between the total flow rate Q_{in} and the total current I_{tot} provides insight into the stability of the flow. If the ratio $Q_{\mathrm{in}}/I_{\mathrm{tot}}$ is small, then the arc develops a steady, uniform, and axisymmetric attachment along the anode surface. For larger ratios, despite the axisymmetry and constancy of boundary conditions, the arc develops a constricted anode attachment and a quasi-periodic movement of the arc is established. For even larger ratios, the arc displays chaotic dynamics (Ref 66-68). These characteristics are often referred as the steady, takeover, and restrike modes of operation of the torch (Ref 69, 70).

The dynamics of the arc inside the torch play a primary role in the flow of the plasma jet. The arc dynamics are a consequence of the unstable imbalance between the Lorentz force exerted over the arc due to the distribution of current density connecting the anode and cathode attachments, and the drag caused by the relatively cold and dense stream of inflow working gas over the hot and low-density arc plasma. The force imbalance causes the dragging of the anode attachment, the elongation of the arc, and the increase in arc curvature until the arc gets in close proximity to another location over the anode. If part of the arc reaches a location near the anode that is closer to the cathode than the current anode attachment, the arc will tend to re-attach, hence forming a new attachment. This phenomenon is known as the arc re-attachment process (Ref 37, 69, 71, 72). This re-attachment is most likely characteristic of the takeover mode of operation of the torch; arc re-attachment in the restrike mode of operation may be driven by different mechanisms, such as breakdown of the cold gas boundary layer or electron avalanches (Ref 69, 70).

The results in Fig. 9 show the evolution of flow through an arc re-attachment process by a set of snapshots of the isosurfaces of T_h = 10 kK and 20 kK at different times, colored by the value of the effective electric potential ϕ_p, using the VMS method. The spacing in between each time is approximately 10 µs. Frame 1 of Fig. 9 (time t_1) shows the initial position of the arc; as the gas pushed the arc downstream (t_2, t_3), the bending of the arc increases, and so does the $\mathbf{J}_q \times \mathbf{B}$ force. The curving of the arc places it close to the anode surface opposite to the current attachment, which leads to an electrical breakdown across the thin layer of cold gas between the arc and the anode, and a new attachment forms in the location indicated by the white arrow at time t_4. The rapid change in the solution during the arc re-attachment process required a reduction in the time step size of between 1 and 2 orders of magnitude and often produced several time step failures (requiring re-initialization of the step with a smaller step size).

To evaluate VMS$_n$ against VMS, Fig. 10 shows sample instantaneous distributions of the heavy-specious temperature T_h, the non-equilibrium parameter θ, and the magnitude of velocity $\|\mathbf{u}\|$ for the times t_2 and t_3 in Fig. 9. The results in Fig. 10 show that the formation of the cathode jet, the dynamics of the arc inside the torch, the development of shear instabilities along the emerging jet, and the development of turbulence along the jet are well captured by both the VMS and VMS$_n$ methods. Interestingly, Fig. 10 shows very little difference between the results obtained with the VMS and VMS$_n$ methods. The incompressible flow simulations (e.g., Fig. 5) showed that VMS$_n$ is more capable of capturing the development of turbulent than VMS. Nevertheless, although it could be expected to see the same trend for the compressible flow simulations, Fig. 6 and 7 show no significant difference between the results using VMS and VMS$_n$ methods. The similarity between results is likely due to the laminarization of the flow due to the heating of gas and consequent increase in viscosity. The results in Fig. 10 indicate that, while both the VMS and VMS$_n$ methods are able to reproduce the main experimentally observed flow dynamics of the arc and jet, there is no significant difference between their prediction of the onset of turbulence. This result implies that the smallest size of eddies captured with VMS$_n$ is comparable to those captured with VMS. The reason for this behavior can be partially explained by investigating the effect of the size of the computational grid on the obtained results using Kolmogorov's turbulence theory (Ref 53).

Kolmogorov's theory indicates the existence of a so-called *inertial* sub-range in fully developed turbulent incompressible flows. The scales of the flow within this sub-range are smaller than the ones directly affected by macroscopic parameters (i.e., domain geometry, boundary conditions), but larger than the scales dominated by molecular dissipation (i.e., viscosity). If the grid is selected such that it is able to resolve the scales within the inertial sub-range, then the results are primarily dependent on the accuracy of the small-scale model. The fact that VMS and VMS$_n$ produced qualitatively the same results for the simulation of the flow from an arc plasma torch may be due to either the computational grid used was too coarse to resolve the inertial sub-range, or the grid was fine enough such that the small scales modeled were well at the end of the inertial sub-range such that the specific model of the small scales is of small relevance. The analysis by Shigeta (Ref 14) indicates that the core of the plasma jet is likely laminar while its surroundings can likely develop instabilities and turbulence. The results in Fig. 10 show a laminar jet core and the development of shear instabilities in the jet periphery, but not the level shown in Fig. 5.

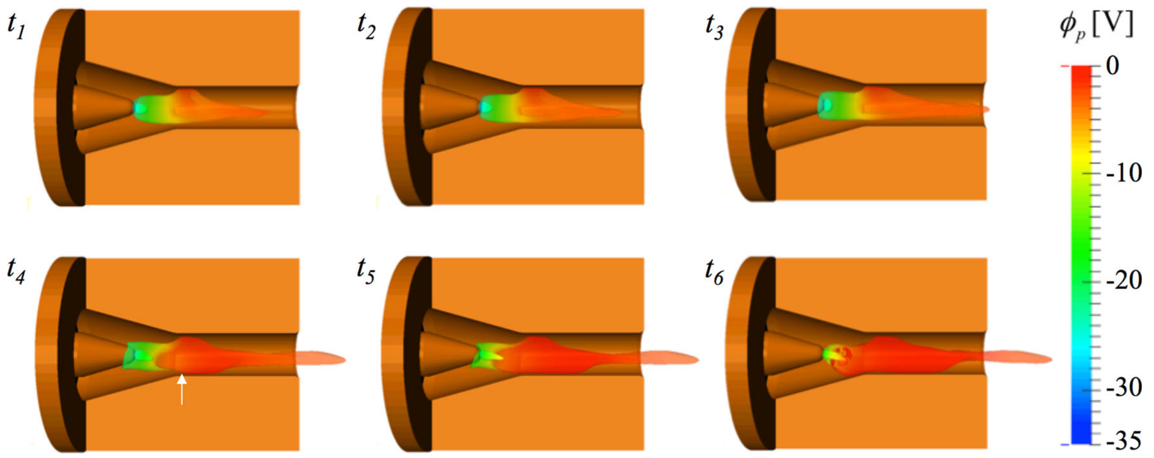

Fig. 9 Temporal sequence of the arc re-attachment process: isosurfaces of heavy-species temperature (10 and 20 kK) across the torch, colored by the value of the effective electric potential ϕ_p. The initial location of the new attachment is indicated with a white arrow

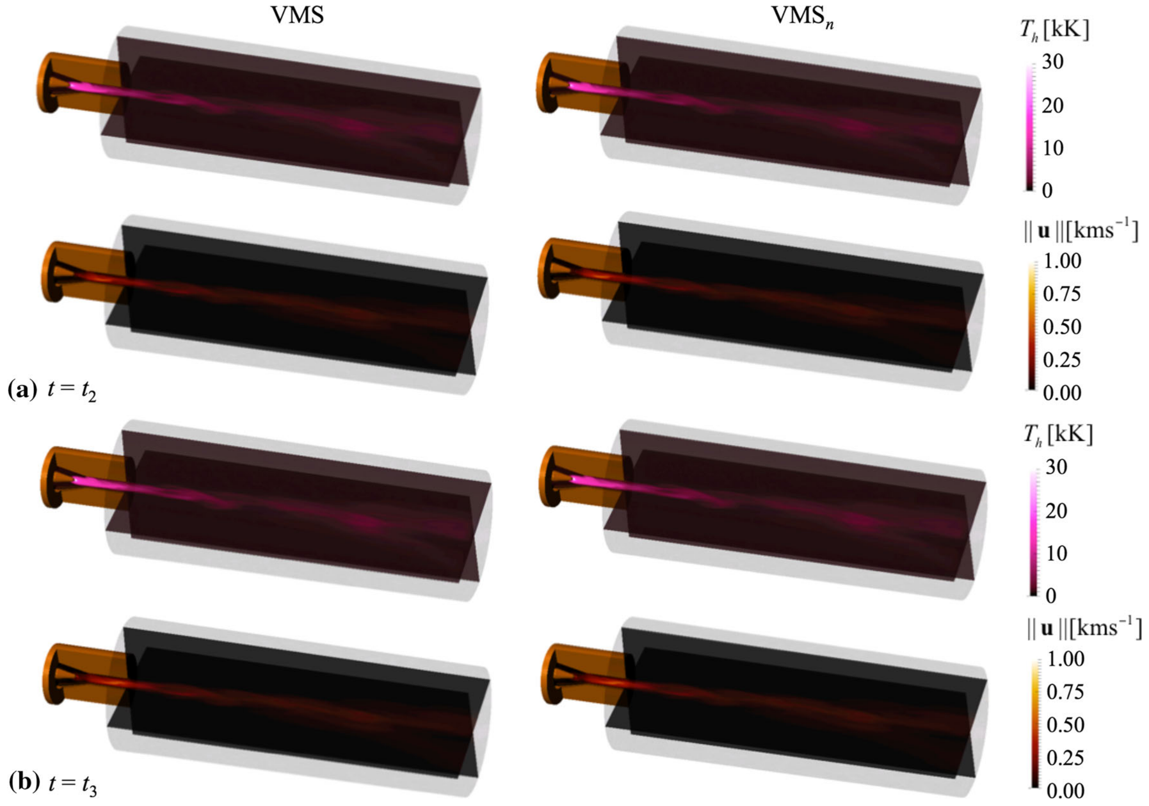

Fig. 10 Comparison between results from the VMS and VMS_n methods: instantaneous distribution of heavy-species temperature and velocity magnitude for two different time instants: (a) t_2 and (b) t_3

Therefore, the accurate description of the flow surrounding the jet requires a significantly finer mesh suitable to resolve the inertial sub-range. Further investigation of the effect of varying spatial and temporal discretization in the results by both methods is needed to verify this result and to further establish the degree of resolution required by comprehensive laminar-to-turbulent flow torch simulations.

Summary and Conclusions

Non-transferred arc torches are at the core of diverse applications, particularly plasma spray. The flow in these torches, particularly at industrially relevant conditions, often transitions from laminar within the torch to turbulent in the emerging jet, and presents significant deviations from local thermodynamic equilibrium (i.e., non-LTE or NLTE). The turbulent nature of the flow, which augments cold-flow entrainment and gas mixing, can drastically affect the degree of non-equilibrium. This fact prompts desirable the use of NLTE models as comprehensive modeling approaches according to their capability to capture both, laminar and turbulent flow regimes. The multiphysics nature of non-equilibrium plasma flows, their inherent high nonlinearity, and the large range of intervening scales make their direct computational simulation, following what is known as direct numerical simulation, practically unfeasible. This fact prompts the need for comprehensive coarse-grained modeling techniques that seek to resolve the large scales of the flow only, while modeling the small scales. Large eddy simulation (LES) techniques are considered the established standard for the exploration of turbulent incompressible flows. Nevertheless, the characteristics of non-equilibrium plasma flow models invalidate the major assumptions in traditional LES models. The flow from a non-transferred torch is simulated using a NLTE plasma flow model solved by a classical variational multiscale (VMS) method and a nonlinear VMS (VMS_n) method. Whereas both methods are suitable for the description of multiscale phenomena, the up-front handling of inter-scale coupling by the VMS_n makes it potentially more suitable for the description of turbulent flows without the need for empirical model parameters. Incompressible (non-plasma) turbulent jet simulations indicate that the VMS_n method produces results comparable to those obtained with the dynamic Smagorinsky method, typically considered the workhorse for turbulent incompressible flow simulations, and significantly more accurate than those by the VMS method. The VMS and VMS_n approaches are applied to the simulation of incompressible, compressible, and NLTE plasma flows in a non-transferred arc torch. The NLTE plasma flow simulations using VMS and VMS_n methods are able to reproduce the dynamics of the arc inside the torch together with the evolution of turbulence in the produced plasma jet in a cohesive manner. However, the similarity of results by both methods indicates the need for numerical resolution significantly higher than what is commonly afforded in arc torch simulations.

Acknowledgment The authors gratefully acknowledge the support from the US National Science Foundation, Division of Physics, through award number PHY-1301935.

References

1. J. Trelles, C. Chazelas, A. Vardelle, and J. Heberlein, Arc Plasma Torch Modeling, *J. Therm. Spray Tech.*, 2009, **18**(5-6), p 728-752
2. F. Mandl, *Statistical Physics*, 2nd ed., Wiley, New York, 2008
3. M.I. Boulos, P. Fauchais, and E. Pfender, *Thermal Plasmas: Fundamentals and Applications*, Plenum Press, Berlin, 1994
4. M.A. Lieberman and A.J. Lichtenberg, *Principles of Plasma Discharges and Materials Processing*, Wiley, New York, 2005
5. T. Matsumoto, D. Wang, H. Akiyama, and T. Namihira, *Non-thermal Plasma Technic for Air Pollution Control*, INTECH Open Access Publisher, Cambridge, 2012
6. P.L. Similon and R.N. Sudan, Plasma Turbulence, *Annu. Rev. Fluid Mech.*, 1990, **22**(1), p 317-347
7. N.B. Volkov, A Model of Two-Temperature Plasma with Strong Large-Scale Turbulence: Dynamic Equations, Thermodynamics and Transport Coefficients, *Plasma Phys. Control. Fusion*, 1999, **41**(11), p 1025-1041
8. M. Shigeta, Turbulence Modelling of Thermal Plasma Flows, *J. Phys. D Appl. Phys.*, 2016, **49**(49), Art ID 493001
9. C. Hackett and G. Settles, *The High-Velocity Oxy-Fuel (HVOF) Thermal Spray-Materials Processing from a Gas Dynamics Perspective, Fluid Dynamics Conference*. American Institute of Aeronautics and Astronautics, 1995
10. A. Vardelle, C. Moreau, N.J. Themelis, and C. Chazelas, A Perspective on Plasma Spray Technology, *Plasma Chem. Plasma Process.*, 2015, **35**(3), p 491-509
11. E. Pfender, J. Fincke, and R. Spores, Entrainment of Cold Gas into Thermal Plasma Jets, *Plasma Chem. Plasma Process.*, 1991, **11**(4), p 529-543
12. J. Hlína, F. Chvála, J. Šonský, and J. Gruber, Multi-Directional Optical Diagnostics of Thermal Plasma Jets, *Meas. Sci. Technol.*, 2008, **19**(1), Art ID 015407
13. J. Hlína, J. Gruber, and J. Šonský, Application of a CCD Camera to Investigations of Oscillations in a Thermal Plasma Jet, *Meas. Sci. Technol.*, 2006, **17**(4), Art ID 918
14. J. Hlína and J. Šonský, Time-Resolved Tomographic Measurements of Temperatures in a Thermal Plasma Jet, *Phys. D Appl. Phys.*, 2010, **43**(5), Art ID 055202
15. J. Hlína, J. Šonský, V. Něnička, and A. Zachar, Statistics of Turbulent Structures in a Thermal Plasma Jet, *Phys. D Appl. Phys.*, 2005, **38**(11), Art ID 1760
16. J.V. Dijk, G.M.W. Kroesen, and A. Bogaerts, Plasma Modelling and Numerical Simulation, *J. Phys. D Appl. Phys.*, 2009, **42**(19), Art ID 190301
17. B.E. Launder and D.B. Spalding, The Numerical Computation of Turbulent Flows, *Comput. Method Appl.*, 1974, **3**(2), p 269-289
18. J.M. Bauchire, J.J. Gonzalez, and A. Gleizes, Modeling of a DC Plasma Torch in Laminar and Turbulent Flow, *Plasma Chem. Plasma Process.*, 1997, **17**(4), p 409-432
19. J. McKelliget, J. Szekely, M. Vardelle, and P. Fauchais, Temperature and Velocity Fields in a Gas Stream Exiting a Plasma Torch. A Mathematical Model and Its Experimental Verification, *Plasma Chem. Plasma Process.*, 1982, **2**(3), p 317-332
20. L. He-Ping and C. Xi, Three-Dimensional Modelling of a DC Non-transferred Arc Plasma Torch, *Phys. D Appl. Phys.*, 2001, **34**(17), Art ID L99
21. L. He-Ping and E. Pfender, Three-Dimensional Effects Inside a DC Arc Plasma Torch, *IEEE Therm. Plasma Sci.*, 2005, **33**(2), p 400-401
22. R. Huang, H. Fukanuma, Y. Uesugi, and Y. Tanaka, Simulation of Arc Root Fluctuation in a DC Non-transferred Plasma Torch with Three Dimensional Modeling, *J. Therm. Spray Technol.*, 2012, **21**(3), p 636-643
23. R. Huang, H. Fukanuma, Y. Uesugi, and Y. Tanaka, An Improved Local Thermal Equilibrium Model of DC Arc Plasma Torch, *IEEE Therm. Plasma Sci.*, 2011, **39**(10), p 1974-1982
24. X.Q. Yuan, H. Li, T.Z. Zhao, F. Wang, W.K. Guo, and P. Xu, Comparative Study of Flow Characteristics Inside Plasma Torch with Different Nozzle Configurations, *Plasma Chem. Plasma Process.*, 2004, **24**(4), p 585-601
25. X.Q. Yuan, T.Z. Zhao, W.K. Guo, and P. Xu, Plasma Flow Characteristics Inside the Supersonic DC Plasma Torch, *Int. J. Mod. Phys. A*, 2005, **14**(02), p 225-238

26. Z. Guo, S. Yin, H. Liao, and S. Gu, Three-Dimensional Simulation of an Argon-Hydrogen DC Non-transferred Arc Plasma Torch, *Int. J. Heat Mass Trans.*, 2015, **80**(3), p 644-652
27. A. Sahai, N.N. Mansour, B. Lopez, and M. Panesi, Modeling of High Pressure Arc-Discharge With a Fully-Implicit Navier–Stokes Stabilized Finite Element Flow Solver, *Plasma Sour. Sci. Technol.*, 2017, **26**(5), Art ID 055012
28. E. Ghedini and V. Colombo, Time Dependent 3D Large Eddy Simulation of a DC Non-Transferred Arc Plasma Spraying Torch with Particle Injection, in *2007 IEEE 34th International Conference on Plasma Science (ICOPS), 17-22 June 2007, 2007*, pp 899-899
29. C. Caruyer, S. Vincent, E. Meillot, J.-P. Caltagirone, and D. Damiani, Analysis of the Unsteadiness of a Plasma Jet and the Related Turbulence, *Surf. Coat. Technol.*, 2010, **205**(4), p 1165-1170
30. S.M. ModirKhazeni and J. Trelles, Towards a Comprehensive Modelling and Simulation Approach for Turbulent Non-equilibrium Plasma Flows, in *22th International Symposium on Plasma Chemistry*, 2015
31. S.M. Modirkhazeni and J.P. Trelles, Preliminary Results of a Consistent and Complete Approach for the Coarse-Grained Simulation of Turbulent Nonequilibrium Plasmas, in *Gordon Research Conference on Plasma Processing Science*, 2016
32. S.M. Modirkhazeni and J.P. Trelles, Algebraic Approximation of Sub-Grid Scales for the Variational Multiscale Modeling of Transport Problems, *Comput. Method Appl. Mech.*, 2016, **306**, p 276-298
33. J.P. Trelles and S.M. Modirkhazeni, Variational Multiscale Method for Non-equilibrium Plasma Flows, *Comput. Method Appl. Mech.*, 2014, **282**, p 87-131
34. L. Arkeryd, On the Boltzmann Equation Part II: The Full Initial Value Problem, *Arch. Ration. Mech. Anal.*, 1972, **45**(1), p 17-34 (in English)
35. J. Trelles, E. Pfender, and J. Heberlein, Multiscale Finite Element Modeling of Arc Dynamics in a DC Plasma Torch, *Plasma Chem. Plasma Process.*, 2006, **26**(6), p 557-575 (in English)
36. J.P. Trelles, E. Pfender, and J.V.R. Heberlein, Thermal Non-equilibrium Simulation of an Arc Plasma Jet, *IEEE Therm. Plasma Sci.*, 2008, **36**(4), p 1026-1027
37. J. Trelles, J. Heberlein, and E. Pfender, Non-equilibrium Modelling of Arc Plasma Torches, *Phys. D Appl. Phys.*, 2007, **40**(19), Art ID 5937
38. G. Hauke and T.J.R. Hughes, A Comparative Study of Different Sets of Variables for Solving Compressible and Incompressible Flows, *Comput. Method Appl. Mech.*, 1998, **153**(1-2), p 1-44
39. S. Chapman and T.G. Cowling, *The Mathematical Theory of Non-uniform Gases: An Account of the Kinetic Theory of Viscosity, Thermal Conduction and Diffusion in Gases*, Cambridge University Press, Cambridge, 1970
40. J.D. Ramshaw and C.H. Chang, Multicomponent Diffusion in Two-Temperature Magnetohydrodynamics, *Phys. Rev. E*, 1996, **53**(6), p 6382-6388
41. J.P. Trelles, Finite Element Methods for Arc Discharge Simulation, *Plasma Process. Polym.*, 2017, **14**(1-2), Art ID 1600092
42. V. Rat, P. André, J. Aubreton, M.F. Elchinger, P. Fauchais, and D. Vacher, Transport Coefficients Including Diffusion in a Two-Temperature Argon Plasma, *Phys. D Appl. Phys.*, 2002, **35**(10), Art ID 981
43. J. Menart, J. Heberlein, and E. Pfender, Theoretical Radiative Transport Results for a Free-Burning Arc Using a Line-By-Line Technique, *J. Phys. D Appl. Phys.*, 1999, **32**(1), Art ID 55
44. F. Lago, J.J. Gonzalez, P. Freton, and A. Gleizes, A Numerical Modelling of an Electric Arc and Its Interaction with the Anode: Part I. The Two-Dimensional Model, *J. Phys. D Appl. Phys.*, 2004, **37**(6), Art ID 883
45. A.A. Iordanidis and C.M. Franck, Self-Consistent Radiation-Based Simulation of Electric Arcs: II. Application to Gas Circuit Breakers, *J. Phys. D Appl. Phys.*, 2008, **41**(13), Art ID 135206
46. J.J. Lowke, Predictions of Arc Temperature Profiles using Approximate Emission Coefficients for Radiation Losses, *J. Quant. Spectrosc. Radiat.*, 1974, **14**(2), p 111-122
47. J. Menart and S. Malik, Net Emission Coefficients for Argon-Iron Thermal Plasmas, *J. Phys. D Appl. Phys.*, 2002, **35**(9), Art ID 867
48. Y. Naghizadeh-Kashani, Y. Cressault, and A. Gleizes, Net Emission Coefficient of Air Thermal Plasmas, *J. Phys. D Appl. Phys.*, 2002, **35**(22), Art ID 2925
49. J.P. Trelles, Computational Study of Flow Dynamics From a DC Arc Plasma Jet, *Phys. D Appl. Phys.*, 2013, **46**(25), Art ID 255201
50. R. Codina, Stabilized Finite Element Approximation of Transient Incompressible Flows Using Orthogonal Subscales, *Comput. Methods Appl. Mech. Eng.*, 2002, **191**(39-40), p 4295-4321
51. T.J.R. Hughes and G. Sangalli, Variational Multiscale Analysis: The Fine-Scale Green's Function, Projection, Optimization, Localization, and Stabilized Methods, *Soc. Ind. Appl. Math. J. Numer. Anal.*, 2007, **45**(2), p 539-557
52. T.J.R. Hughes and G. Sangalli, Variational Multiscale Analysis: The Fine-Scale Green's Function, Projection, Optimization, Localization, and Stabilized Methods, *SIAM J. Numer. Anal.*, 2007, **45**(2), p 539-557
53. R. Codina, On Stabilized Finite Element Methods for Linear Systems of Convection–Diffusion–Reaction Equations, *Comput. Method Appl. Mech.*, 2000, **188**(1), p 61-82
54. T.J.R. Hughes, G. Scovazzi, and T.E. Tezduyar, Stabilized Methods for Compressible Flows, *J. Sci. Comput.*, 2010, **43**(3), p 343-368 (in English)
55. F. Rispoli and G.Z. Rafael Saavedra, A Stabilized Finite Element Method Based on SGS Models for Compressible Flows, *Comput. Method Appl. Mech.*, 2006, **196**(1-3), p 652-664
56. TPORT, http://faculty.uml.edu/Juan_Pablo_Trelles/Software/TPORT.aspx. Accessed 2017.
57. K.E. Jansen, C.H. Whiting, and G.M. Hulbert, A Generalized-α Method for Integrating the Filtered Navier–Stokes Equations with a Stabilized Finite Element Method, *Comput. Method Appl. Mech.*, 2000, **190**(3), p 305-319
58. S.C. Eisenstat and H.F. Walker, Choosing the Forcing Terms in an Inexact Newton Method, *SIAM J. Sci. Comput.*, 1996, **17**(1), p 16-32
59. S.J. Kwon and I.W. Seo, Reynolds Number Effects on the Behavior of a Non-buoyant Round Jet, *Exp. Fluids*, 2005, **38**(6), p 801-812
60. K.B.M.Q. Zaman and A.K.M.F. Hussain, Vortex Pairing in a Circular Jet Under Controlled Excitation. Part 1. General Jet Response, *J. Fluid Mech.*, 1980, **101**(3), p 449-491
61. M. Germano, U. Piomelli, P. Moin, and W.H. Cabot, A Dynamic Subgrid-Scale Eddy Viscosity Model, *Phys. Fluids Fluid Dyn.*, 1991, **3**(7), p 1760-1765
62. D.K. Lilly, A Proposed Modification of the Germano Subgrid-Scale Closure Method, *Phys. Fluids Fluid Dyn.*, 1992, **4**(3), p 633-635
63. Fluent, Ansys Inc. http://www.ansys.com/Products/Simulation+Technology/Fluid+Dynamics/Fluid+Dynamics+Products/ANSYS+Fluent. Accessed 2017.
64. V.M. Tikhomirov, *Dissipation of Energy in Isotropic Turbulence, Selected Works*, A.N. Kolmogrov and V.M. Tikhomirov, Ed., Springer, Amsterdam, 1991, p 324-327
65. K.C. Hsu and E. Pfender, Two-Temperature Modeling of the Free-Burning, High-Intensity Arc, *J. Appl. Phys.*, 1983, **54**(8), p 4359-4366
66. Z. Duan and J. Heberlein, Arc Instabilities in a Plasma Spray Torch, *J. Therm. Spray Technol.*, 2002, **11**(1), p 44-51

67. P. Fauchais, Understanding Plasma Spraying, *J. Phys. D Appl. Phys.*, 2004, **37**(9), Art ID R86
68. E. Moreau, C. Chazelas, G. Mariaux, and A. Vardelle, Modeling the Restrike Mode Operation of a DC Plasma Spray Torch, *J. Therm. Spray Technol.*, 2006, **15**(4), p 524-530
69. C. Chazelas, J.P. Trelles, I. Choquet, and A. Vardelle, Main Issues for a Fully Predictive Plasma Spray Torch Model and Numerical Considerations, *Plasma Chem. Plasma*, 2017, **37**(3), p 627-651
70. C. Chazelas, J.P. Trelles, and A. Vardelle, The Main Issues to Address in Modeling Plasma Spray Torch Operation, *J. Therm. Spray Technol.*, 2017, **26**(1), p 3-11
71. C. Baudry, A. Vardelle, G. Mariaux, M. Abbaoui, and A. Lefort, Numerical Modeling of a DC Non-transferred Plasma Torch: Movement of the Arc Anode Attachment and Resulting Anode Erosion, *Int. Quart. High Technol. Plasma Processs.*, 2005, **9**(1), p 1-15
72. J.P. Trelles, E. Pfender, and J.V.R. Heberlein, Modelling of the Arc Reattachment Process in Plasma Torches, *Phys. D Appl. Phys.*, 2007, **40**(18), Art ID 5635